Δ-mediated pion production in nuclei

C. Praet,* O. Lalakulich,† N. Jachowicz, and J. Ryckebusch
Department of Subatomic and Radiation Physics, Ghent University, Proeftuinstraat 86, B-9000 Gent, Belgium
(Received 17 April 2008; revised manuscript received 22 December 2008; published 9 April 2009)

We present a fully relativistic formalism for describing neutrino-induced Δ-mediated single-pion production in nuclei. We assess the ambiguities stemming from the Δ interactions and quantify the uncertainties in the axial form-factor parameters by comparing with the available bubble-chamber neutrino-scattering data. To include nuclear effects, we turn to a relativistic plane-wave impulse approximation (RPWIA) using realistic bound-state wave functions derived in the Hartree approximation to the σ-ω Walecka model. For neutrino energies larger than 1 GeV, we show that a relativistic Fermi-gas model with appropriate binding-energy correction produces results that are comparable to the RPWIA that naturally includes Fermi motion, nuclear-binding effects, and the Pauli exclusion principle. Including Δ medium modifications roughly halves the RPWIA cross section. Calculations for *primary* (prior to undergoing final-state interactions) pion production are presented for both electron- and neutrino-induced processes, and a comparison with electron-scattering data and other theoretical approaches is included. We infer that the total Δ-production strength is underestimated by about 20 to 25%, a fraction that is due to the pionless decay modes of the Δ in a medium. The model presented in this work can be naturally extended to include the effect of final-state interactions in a relativistic and quantum-mechanical way.

DOI: 10.1103/PhysRevC.79.044603 PACS number(s): 25.30.Pt, 13.15.+g, 21.60.−n, 24.10.Jv

I. INTRODUCTION

In the past few years, precision measurements of the neutrino-oscillation parameters have driven the interest in medium-energy neutrino physics. The MiniBooNE [1] and K2K [2] Collaborations have recently collected a wealth of neutrino data in the 1-GeV energy range [3–8], where the vast part of the strength can be attributed to quasielastic (QE) processes and Δ-mediated one-pion production. A thorough understanding of these cross sections is essential to reduce the systematic uncertainties. In turn, the high-statistics data from these and future neutrino experiments like MINERνA [9] and SciBooNE [10] offer the opportunity to address a variety of topics related to hadronic and nuclear weak physics.

Various theoretical models have been developed to study one-pion production on a free nucleon [11–20]. These efforts chiefly focus on studying the vector and axial-vector form factors that are introduced to parametrize the incomplete knowledge of the Δ-production vertex. Whereas the vector form factors can be well determined from electroproduction data [15,17], the axial-vector ones remain troublesome due to the large error flags present in early bubble-chamber neutrino data and sizable model dependencies in their analyses [20,21]. Moreover, various theoretical calculations of the most important axial form factor, $C_5^A(Q^2)$, reveal highly different pictures [22–27]. Consequently, the Q^2 evolution of the axial form factors and the axial one-pion mass M_A are rather poorly known. Concerning the Δ-decay vertex, it has been established that the traditionally used decay couplings are not fully consistent with the Rarita-Schwinger field-theoretic description of the Δ particle [28]. Instead, one can construct a consistent interaction that couples solely to the physical spin-3/2 part of the Δ propagator [28]. Because planned neutrino-scattering experiments aim at putting further constraints on M_A and the axial form factors, it is important to assess the ambiguities related to the incomplete knowledge of the Δ interactions.

The extraction of M_A and the axial form factors is made even more challenging by the fact that nuclei are employed as detectors. Thus, various nuclear effects need to be addressed to make realistic cross-section predictions. Traditionally, the Fermi motion of the nucleons inside the nucleus is described within the relativistic Fermi gas (RFG) [29,30]. Owing to its relative simplicity, the RFG model has been the preferred nuclear model in neutrino-event generators. Going beyond the RFG, realistic bound-state wave functions can be calculated within a relativistic shell model [30,31] or by using spectral functions that extend beyond the mean-field picture [32–35]. A comparison of these models provides insight into the nuclear-model dependence of the computed cross sections. Another nuclear effect stems from the fact that the Δ properties are modified in a medium [36], generally resulting in a shift of the peak position and a collisional broadening of the width. The effect of Δ medium modifications on neutrino-induced cross sections has been studied in Refs. [37,38] and also, more recently, in Refs. [39–42]. Finally, one must consider the final-state interactions (FSI) of the outgoing pion and nucleon. To study the effect of FSI, recent efforts have adopted semiclassical and Monte Carlo techniques [39,40]. Based on these results, it is clear that FSI mechanisms produce by far the largest nuclear effect on one-pion production computations.

In this work, we focus on the neutrino-induced charged-current one-pion production process. Thereby, we assume that all produced pions originate from the decay of a Δ resonance, i.e., we adhere to the Δ dominance model. First,

*christophe.praet@ugent.be
†Present address: Institut für Theoretische Physik, Universität Giessen, Germany.

the sensitivity of the cross section to uncertainties in the Δ couplings is assessed. To this end, we compare computations using different axial-vector form factors with the available Argonne National Laboratory (ANL) and Brookhaven National Laboratory (BNL) cross-section data. This makes it possible to make statements about the present uncertainty on these cross sections, which is of great relevance for the analysis of neutrino-oscillation experiments.

Turning to nuclear targets, we present a fully relativistic formalism that can serve as a starting point to investigate Δ-mediated one-pion production from nuclei. Recognizing the ability of the new generation of experiments to measure both inclusive and semi-inclusive observables, we develop a framework that is geared toward a detailed study of various distributions, like Q^2, W, energy, and scattering-angle dependences. More specifically, this article deals with the description of *primary* Δ-mediated one-pion production in nuclei, and its relation to inclusive observables. Hence, a discussion of FSI mechanisms, which is definitely required in computations of semi-inclusive observables like pion-energy distributions, falls beyond the scope of this text. To model nuclear effects, we turn to the relativistic plane-wave impulse approximation, using relativistic bound-state wave functions that are calculated in the Hartree approximation to the σ-ω Walecka model [43]. This approach was successfully applied in QE nucleon-knockout studies [31,44–46] and includes the effects of Fermi motion, nuclear binding, and the Pauli exclusion principle in a natural way. Medium modifications of the Δ particle are taken into account along the lines of Ref. [36]. We investigate the nuclear-model dependence of our results, by comparing with RFG calculations. Our findings in this regard are of great interest to neutrino experiments that employ the RFG model in their event generators. Finally, we show our computations for the Δ-mediated one-pion yield and compare them to other theoretical approaches and electron-scattering data.

The article is organized as follows. Section II introduces the formalism for the elementary Δ-mediated one-pion production process. The third section deals with the nuclear model and discusses the framework for the description of neutrino-nucleus interactions. Numerical results are presented in Sec. IV. In Sec. V, we summarize our conclusions.

II. WEAK ONE-PION PRODUCTION ON THE NUCLEON

A. Cross section

For a free proton target, the charged-current (CC) process under study is

$$\nu_\mu + p \overset{\Delta^{++}}{\rightarrow} \mu^- + p + \pi^+. \tag{1}$$

The corresponding reactions for a free neutron are

$$\begin{aligned} \nu_\mu + n &\overset{\Delta^{+}}{\rightarrow} \mu^- + p + \pi^0, \\ \nu_\mu + n &\overset{\Delta^{+}}{\rightarrow} \mu^- + n + \pi^+. \end{aligned} \tag{2}$$

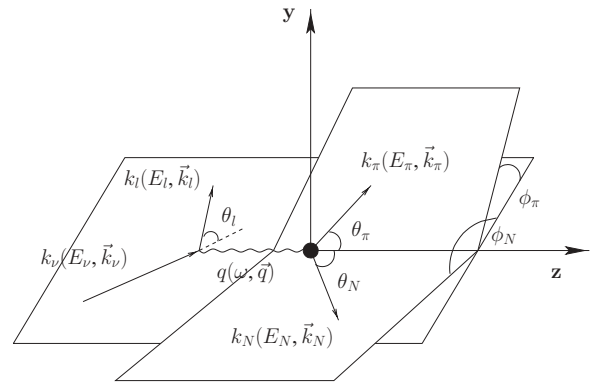

FIG. 1. Kinematics for neutrino-induced charged-current one-pion production on the nucleon.

Isospin considerations allow one to relate the strength of the above reactions

$$\begin{aligned} \sigma(W^+ p \overset{\Delta^{++}}{\rightarrow} p\pi^+) &= 9\sigma(W^+ n \overset{\Delta^{+}}{\rightarrow} n\pi^+) \\ &= \tfrac{9}{2}\sigma(W^+ n \overset{\Delta^{+}}{\rightarrow} p\pi^0), \end{aligned} \tag{3}$$

where W^+ denotes the exchanged weak vector boson. In a laboratory frame of reference, the corresponding differential cross section is given by [47]

$$\begin{aligned} d^9\sigma = &\frac{1}{\beta}\frac{m_\nu}{E_\nu}\frac{m_l}{E_l}\frac{d^3\vec{k}_l}{(2\pi)^3}\frac{m_N}{E_N}\frac{d^3\vec{k}_N}{(2\pi)^3}\frac{d^3\vec{k}_\pi}{2E_\pi(2\pi)^3}\overline{\sum}_{fi}\left|M_{fi}^{(\text{free})}\right|^2 \\ &\times (2\pi)^4\delta^{(4)}(k_\nu + k_{N,i} - k_l - k_\pi - k_N). \end{aligned} \tag{4}$$

Figure 1 defines our conventions for the kinematical variables. The target nucleon has four-momentum $k_{N,i} = (m_N, \vec{0})$, with m_N the nucleon's mass. We write $k_\nu = (E_\nu, \vec{k}_\nu)$ for the incoming neutrino, $k_l = (E_l, \vec{k}_l)$ for the outgoing muon, $k_\pi = (E_\pi, \vec{k}_\pi)$ for the outgoing pion and $k_N = (E_N, \vec{k}_N)$ for the outgoing nucleon. The xyz coordinate system is chosen such that the z axis lies along the momentum transfer $\vec{q}$, the y axis along $\vec{k}_\nu \times \vec{k}_l$, and the x axis in the lepton-scattering plane. In Eq. (4), the incoming neutrino's relative velocity $\beta = |\vec{k}_\nu|/E_\nu$ is 1. The neutrino mass m_ν cancels with the neutrino normalization factor appearing in the lepton tensor. The δ function expresses energy-momentum conservation and $\overline{\sum}_{fi}|M_{fi}^{(\text{free})}|^2$ denotes the squared invariant matrix element, appropriately averaged over initial spins and summed over final spins. Using the δ function to integrate over the outgoing nucleon's three-momentum and the magnitude of the pion's momentum, one arrives at the fivefold cross section

$$\begin{aligned} \frac{d^5\sigma}{dE_l d\Omega_l d\Omega_\pi} = &\frac{m_\nu m_l |\vec{k}_l| m_N |\vec{k}_\pi|}{2(2\pi)^5 E_\nu |E_N + E_\pi(|\vec{k}_\pi|^2 - \vec{q}\cdot\vec{k}_\pi)/|\vec{k}_\pi|^2|} \\ &\times \overline{\sum}_{fi}\left|M_{fi}^{(\text{free})}\right|^2, \end{aligned} \tag{5}$$

where the solid angles Ω_l and Ω_π define the direction of the outgoing muon and pion, respectively.

B. Matrix element for resonant one-pion production

Next to the kinematic phase-space factor, Eq. (5) contains the squared invariant matrix element

$$\overline{\sum}_{fi}\left|M_{fi}^{(\mathrm{free})}\right|^2=\frac{1}{2}\sum_{\substack{s_\nu;s_l\\ s_{N,i};s_N}}\left[M_{fi}^{(\mathrm{free})}\right]^\dagger M_{fi}^{(\mathrm{free})}. \tag{6}$$

Here, the sum over final muon and nucleon spins is taken. Averaging over the initial nucleon's spin, $s_{N,i}$, leads to a factor $1/2$. An explicit expression for the invariant matrix element is obtained by applying the Feynman rules in momentum space. Writing

$$M_{fi}^{(\mathrm{free})}=i\frac{G_F\cos\theta_c}{\sqrt{2}}\left\langle J_{\mathrm{had}}^{\rho(\mathrm{free})}\right\rangle S_{W,\rho\sigma}\left\langle J_{\mathrm{lep}}^{\sigma}\right\rangle, \tag{7}$$

with G_F the Fermi constant and θ_c the Cabibbo angle, one distinguishes the hadron current

$$\left\langle J_{\mathrm{had}}^{\rho(\mathrm{free})}\right\rangle=\overline{u}(k_N,s_N)\Gamma^{\mu}_{\Delta\pi N}S_{\Delta,\mu\nu}\Gamma^{\nu\rho}_{WN\Delta}u(k_{N,i},s_{N,i}), \tag{8}$$

the weak boson propagator

$$S_{W,\rho\sigma}=\frac{g_{\rho\sigma}M_W^2}{Q^2+M_W^2};\quad Q^2=-q_\mu q^\mu, \tag{9}$$

and the lepton current

$$\left\langle J_{\mathrm{lep}}^{\sigma}\right\rangle=\overline{u}(k_l,s_l)\gamma^\sigma(1-\gamma_5)u(k_\nu,s_\nu). \tag{10}$$

Clearly, the least-known physics is contained in the vertex functions of the matrix element of Eq. (8). For the Δ-production vertex, we adopt the form [12]

$$\begin{aligned}\Gamma^{\nu\rho}_{WN\Delta}(k_\Delta,q)=&\left[\frac{C_3^V(Q^2)}{m_N}(g^{\nu\rho}\not{q}-q^\nu\gamma^\rho)\right.\\&+\frac{C_4^V(Q^2)}{m_N^2}\left(g^{\nu\rho}q\cdot k_\Delta-q^\nu k_\Delta^\rho\right)\\&+\frac{C_5^V(Q^2)}{m_N^2}\left(g^{\nu\rho}q\cdot k_{N,i}-q^\nu k_{N,i}^\rho\right)\\&\left.+g^{\nu\rho}C_6^V(Q^2)\right]\gamma_5+\frac{C_3^A(Q^2)}{m_N}(g^{\nu\rho}\not{q}-q^\nu\gamma^\rho)\\&+\frac{C_4^A(Q^2)}{m_N^2}\left(g^{\nu\rho}q\cdot k_\Delta-q^\nu k_\Delta^\rho\right)\\&+C_5^A(Q^2)g^{\nu\rho}+\frac{C_6^A(Q^2)}{m_N^2}q^\nu q^\rho,\end{aligned} \tag{11}$$

which relates to the $n\to\Delta^+$ transition. The vector ($C_i^V, i=3..6$) and axial ($C_i^A, i=3..6$) form factors that are introduced in Eq. (11) are constrained by physical principles and experimental data. Imposing the conserved vector current (CVC) hypothesis leads to $C_6^V=0$. The partially conserved axial current (PCAC) hypothesis, together with the pion-pole dominance assumption, yields the following relation between C_5^A and the pseudoscalar form factor C_6^A

$$C_6^A=C_5^A\frac{m_N^2}{Q^2+m_\pi^2}. \tag{12}$$

At $Q^2=0$, the off-diagonal Goldberger-Treiman relation gives $C_5^A=1.2$ [13]. Furthermore, CVC entails that the weak vector current and the isovector part of the electromagnetic current are components of the same isospin current. Consequently, after extracting the electromagnetic form factors from electroproduction data, the $C_i^V, i=3,4,5$ follow immediately by applying the appropriate transformations in isospin space. To extract the vector form factors, it has been established that the magnetic-dipole ($M1$) dominance of the electromagnetic $N\to\Delta$ transition amplitude is a reasonable assumption [48]. This $M1$ dominance leads to the conditions [13,49]

$$C_4^V=-C_3^V\frac{m_N}{W},\quad C_5^V=0, \tag{13}$$

where W is the invariant mass, defined as $W=\sqrt{k_\Delta^2}$. For C_3^V, a modified-dipole parametrization is extracted [16,50]

$$C_3^V=\frac{1.95D_V}{1+Q^2/4M_V^2}, \tag{14}$$

with $D_V=(1+Q^2/M_V^2)^{-2}$ the dipole function and $M_V=0.84$ GeV. In Eq. (14), the faster-than-dipole falloff reflects the fact that the Δ is a more extended object than a nucleon. Within this scheme, it is possible to relate all weak vector form factors to C_3^V. More recently, a direct analysis of the electroproduction helicity amplitudes from JLab and Mainz experiments resulted in an alternative parametrization of the weak vector form factors [17]

$$\begin{aligned}C_3^V&=\frac{2.13D_V}{1+Q^2/4M_V^2},\quad C_4^V=\frac{-1.51}{2.13}C_3^V,\\C_5^V&=\frac{0.48D_V}{1+Q^2/0.776M_V^2},\end{aligned} \tag{15}$$

attributing a nonzero strength to the weak vector form factor C_5^V. The axial form factors are even more difficult to determine, in the sense that they are only constrained by the bubble-chamber neutrino data. A popular parametrization is given by [16,40,50]

$$\begin{aligned}C_5^A&=\frac{1.2}{\left(1+Q^2/M_A^2\right)^2}\frac{1}{1+Q^2/3M_A^2},\\C_4^A&=-\frac{C_5^A}{4},\quad C_3^A=0,\end{aligned} \tag{16}$$

where $M_A=1.05$ GeV. However, there still resides a great deal of uncertainty in the axial form factors or, equivalently, in C_5^A. The extracted axial-mass value, for example, is heavily model dependent [20,21]. A reanalysis [20] of ANL data within a model that includes background contributions next to the Δ-pole mechanism reveals a $C_5^A(0)$ value that is lower than the one predicted by the Goldberger-Treiman relation. This result is corroborated by recent chiral constituent-quark (χCQ) results [22] and lattice QCD calculations [23,24]. Figure 2 compares the two theoretical results with the phenomenological fit of Eq. (16). It can be clearly seen that all three approaches exhibit highly different Q^2 evolutions.

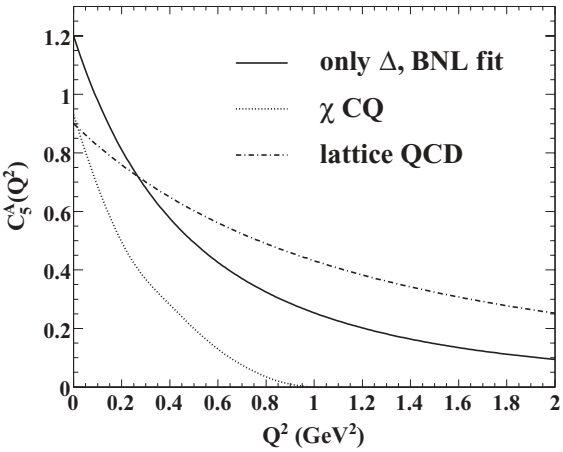

FIG. 2. Results for the axial transition form factor $C_5^A(Q^2)$. The full line represents Eq. (16). The dash-dotted line shows a quenched lattice result and is parameterized as $C_5^A(Q^2) = C_5^A(0)(1 + Q^2/\tilde{M}_A^2)^{-2}$, $C_5^A(0) = 0.9$, and $\tilde{M}_A = 1.5$ GeV [24]. The dotted line corresponds to a χCQ result and is taken from Ref. [22].

The Rarita-Schwinger spin-3/2 propagator for the Δ reads

$$S_{\Delta,\mu\nu}(k_\Delta) = \frac{-(\not{k}_\Delta + M_\Delta)}{k_\Delta^2 - M_\Delta^2 + iM_\Delta\Gamma}\left(g_{\mu\nu} - \frac{\gamma_\mu\gamma_\nu}{3} - \frac{2k_{\Delta,\mu}k_{\Delta,\nu}}{3M_\Delta^2} - \frac{\gamma_\mu k_{\Delta,\nu} - \gamma_\nu k_{\Delta,\mu}}{3M_\Delta}\right), \quad (17)$$

where $M_\Delta = 1.232$ GeV and Γ stands for the free decay width.

A common way of describing the Δ decay is through the interaction Lagrangian

$$\mathcal{L}_{\pi N\Delta} = \frac{f_{\pi N\Delta}}{m_\pi}\overline{\psi}_\mu \vec{T}^\dagger(\partial^\mu\vec{\phi})\psi + \text{h.c.}, \quad (18)$$

where ψ_μ, $\vec{\phi}$, and ψ denote the spin-3/2 Rarita-Schwinger field, the pion field and the nucleon field, respectively. The operator $\vec{T}$ is the isospin $1/2 \to 3/2$ transition operator. From Eq. (18), one derives the vertex function

$$\Gamma^\mu_{\Delta\pi N}(k_\pi) = \frac{f_{\pi N\Delta}}{m_\pi}k_\pi^\mu, \quad (19)$$

and the corresponding energy-dependent width

$$\Gamma(W) = \frac{1}{12\pi}\frac{f_{\pi N\Delta}^2}{m_\pi^2 W}|\vec{q}_{\text{c.m.}}|^3(m_N + E_N), \quad (20)$$

with

$$|\vec{q}_{\text{c.m.}}| = \frac{\sqrt{\left(W^2 - m_\pi^2 - m_N^2\right)^2 - 4m_\pi^2 m_N^2}}{2W}. \quad (21)$$

Requiring that $\Gamma(W = M_\Delta)$ equals the experimentally determined value of 120 MeV, one obtains $f_{\pi N\Delta} = 2.21$. An alternative choice for the $\Delta\pi N$ interaction Lagrangian is provided by

$$\mathcal{L}_{\pi N\Delta} = \frac{f^*_{\pi N\Delta}}{m_\pi M_\Delta}\epsilon^{\alpha\beta\mu\nu}\overline{G}_{\beta\alpha}\gamma_\mu\gamma_5\vec{T}^\dagger(\partial_\nu\vec{\phi})\psi + \text{h.c.}, \quad (22)$$

where $G_{\beta\alpha} = \partial_\beta\psi_\alpha - \partial_\alpha\psi_\beta$. This form has been proposed by Pascalutsa *et al.* [28], who point out that many of the traditional couplings, like the one in Eq. (18), give rise to unwanted spin-1/2 contributions to the cross section. The interaction of Eq. (22), however, couples only to the physical, spin-3/2 part of the Δ propagator. With the interaction Lagrangian of Eq. (22) the vertex function becomes

$$\Gamma^\mu_{\Delta\pi N}(k_\pi, k_\Delta) = \frac{f^*_{\pi N\Delta}}{m_\pi M_\Delta}\epsilon^{\mu\alpha\beta\gamma}k_{\pi,\alpha}\gamma_\beta\gamma_5 k_{\Delta,\gamma}. \quad (23)$$

For on-mass shell Δs, the unphysical spin-1/2 terms are automatically removed by both the Pascalutsa and the traditional couplings. Therefore, calculating the free decay width from Eq. (23) leads to the same expression as in Eq. (20), implying $f^*_{\pi N\Delta} = f_{\pi N\Delta} = 2.21$.

Combining formulas (6) to (10), the squared invariant matrix element can be cast in the form

$$\overline{\sum_{fi}}\left|M_{fi}^{(\text{free})}\right|^2 = \frac{G_F^2\cos^2\theta_c M_W^4}{2\left(M_W^2 + Q^2\right)^2}H^{\rho\sigma}_{(\text{free})}L_{\rho\sigma}, \quad (24)$$

where the leptonic tensor is given by

$$L_{\rho\sigma} = \frac{2}{m_\nu m_l}\left(k_{\nu,\rho}k_{l,\sigma} + k_{\nu,\sigma}k_{l,\rho} - k_\nu\cdot k_l g_{\rho\sigma} - i\epsilon_{\alpha\rho\beta\sigma}k_\nu^\alpha k_l^\beta\right), \quad (25)$$

with the definition $\epsilon_{0123} = +1$. Introducing the shorthand notation $\mathcal{O}^\sigma = \Gamma^\mu_{\Delta\pi N}S_{\Delta,\mu\nu}\Gamma^{\nu\sigma}_{WN\Delta}$, one arrives at the following expression for the hadronic tensor

$$H^{\rho\sigma}_{(\text{free})} = \frac{1}{8m_N^2}\,\text{Tr}\left[(\not{k}_{N,i} + m_N)\widetilde{\mathcal{O}}^\rho(\not{k}_N + m_N)\mathcal{O}^\sigma\right], \quad (26)$$

where $\widetilde{\mathcal{O}}^\rho = \gamma_0(\mathcal{O}^\rho)^\dagger\gamma_0$.

III. WEAK ONE-PION PRODUCTION IN A NUCLEUS

Turning to nuclear targets, a schematical representation of the reaction under study is given by

$$\nu_\mu + A \xrightarrow{\Delta} \mu^- + (A-1) + N + \pi, \quad (27)$$

where A denotes the mass number of the target nucleus. Compared to the free-nucleon case, one now needs to consider the residual nucleus $k_{A-1} = (E_{A-1}, \vec{k}_{A-1})$ as an extra particle in the hadronic final state. Following the same line of reasoning as in Sec. II A, the lab-frame cross section corresponding to the process of Eq. (27) becomes

$$\frac{d^8\sigma}{dE_l d\Omega_l dE_\pi d\Omega_\pi d\Omega_N} = \frac{m_\nu m_l|\vec{k}_l|m_N m_{A-1}|\vec{k}_\pi||\vec{k}_N|}{2(2\pi)^8 E_\nu|E_{A-1} + E_N + E_N\vec{k}_N\cdot(\vec{k}_\pi - \vec{q})/|\vec{k}_N|^2|} \times\overline{\sum_{fi}}\left|M_{fi}^{(\text{bound})}\right|^2. \quad (28)$$

A. Relativistic bound-state wave functions

The invariant matrix element in Eq. (28) carries the tag *bound* and involves nuclear many-body currents between initial and final nuclear wave functions. In medium-energy

physics, however, one usually resorts to a number of assumptions that allow a reduction of the nuclear-current matrix elements to a form similar to Eq. (8). Here, we summarize the main approximations that enable this simplification and refer to Ref. [51] for more detailed considerations. First, we consider only processes where the residual $(A-1)$ system is left with an excitation energy not exceeding a few tens of MeV. The major fraction of the transferred energy is carried by the outgoing pion and nucleon. Further, we adopt the impulse approximation (IA): the nuclear many-body current is replaced by a sum of one-body current operators, exempt from medium effects. Assuming an independent-particle model (IPM) for the initial and final nuclear wave functions, the hadronic current matrix elements can be written in the form of Eq. (8), whereby the initial-nucleon free Dirac spinor is replaced by a bound-state spinor [51]. This approach, where the outgoing nucleon and pion remain unaffected by the nuclear medium, is generally referred to as the relativistic plane-wave impulse approximation (RPWIA).

The single-particle wave functions used in this work are determined in the Hartree approximation to the σ-ω Walecka model, using the $W1$ parametrization for the different field strengths [43]. In the presence of a spherically symmetric potential, the eigenstates of the Dirac equation can be written in a two-component representation as

$$\Psi_{\alpha,m}(\vec{r}) = \begin{bmatrix} i\frac{G(r)}{r}\mathcal{Y}_{+\kappa,m}(\hat{\vec{r}}) \\ -\frac{F(r)}{r}\mathcal{Y}_{-\kappa,m}(\hat{\vec{r}}) \end{bmatrix}, \tag{29}$$

where m is the magnetic quantum number and α stands for all other quantum numbers that specify a single-particle orbital. The functions G and F denote the radial wave functions. In the definition of the spherical two-spinors, a generalized angular momentum κ is introduced. In momentum space, the wave functions are obtained from

$$\mathcal{U}_{\alpha,m}(\vec{p}) = \frac{1}{(2\pi)^{3/2}}\int \Psi_{\alpha,m}(\vec{r})e^{-i\vec{p}\cdot\vec{r}}d\vec{r}. \tag{30}$$

The result is

$$\mathcal{U}_{\alpha,m}(\vec{p}) = i^{(1-l)}\sqrt{\frac{2}{\pi}}\frac{1}{p}\begin{bmatrix} g(p)\mathcal{Y}_{+\kappa,m}(\hat{\vec{p}}) \\ -f(p)\mathcal{Y}_{-\kappa,m}(\hat{\vec{p}}) \end{bmatrix}, \tag{31}$$

with

$$g(p) = \int_0^\infty G(r)\hat{j}_l(pr)dr, \tag{32}$$

and

$$f(p) = \mathrm{sgn}(\kappa)\int_0^\infty F(r)\hat{j}_{\bar{l}}(pr)dr, \qquad \bar{l} = \begin{pmatrix} l+1, & \kappa<0 \\ l-1, & \kappa>0 \end{pmatrix}. \tag{33}$$

In Eqs. (32) and (33), $\hat{j}_l(x) = xj_l(x)$ are the Ricatti-Bessel functions.

Returning to the calculation of the squared invariant matrix element in Eq. (28), the following factor appears

$$S_\alpha(\vec{p}) = \frac{1}{2j+1}\sum_m \mathcal{U}_{\alpha,m}(\vec{p})\overline{\mathcal{U}}_{\alpha,m}(\vec{p}). \tag{34}$$

This expression, referred to as the bound-state propagator, can be cast in a form that is similar to the free-nucleon projection operator [52]. One finds

$$S_\alpha(\vec{p}) = (\not{k}_\alpha + M_\alpha), \tag{35}$$

with the definitions

$$\begin{aligned} M_\alpha &= \frac{1}{(2\pi)^3}\frac{\pi}{p^2}[g^2(p) - f^2(p)], \\ E_\alpha &= \frac{1}{(2\pi)^3}\frac{\pi}{p^2}[g^2(p) + f^2(p)], \\ \vec{k}_\alpha &= \frac{1}{(2\pi)^3}\frac{\pi}{p^2}[2g(p)f(p)\hat{\vec{p}}]. \end{aligned} \tag{36}$$

In other words, the hadronic tensor for scattering off a bound nucleon is readily found from the free-nucleon one in Eq. (26) by making the replacement

$$\frac{1}{2}\frac{(\not{k}_{N,i} + m_N)}{2m_N} \longrightarrow (2\pi)^3(\not{k}_\alpha + M_\alpha). \tag{37}$$

Figure 3 shows the momentum wave functions of Eqs. (32) and (33) for a proton belonging to a specified carbon shell. Due to the small contribution of the lower wave function component, the quantities M_α and E_α are almost equal.

B. Medium modifications of Δ properties

In a nuclear environment, the Δ mass and width are modified with respect to their free values. These medium modifications can be estimated by calculating the in-medium Δ self-energy, as was done, e.g., in Ref. [36]. The real part of the Δ self-energy causes a shift of the resonance position, whereas the imaginary part is related to the decay width. Medium modifications for the width result from the competition between a Pauli-blocking correction, reducing the free decay width, and a term proportional to the imaginary part of the Δ self-energy, including various meson and baryon interaction mechanisms and, therefore, enhancing the free decay width. A convenient parametrization for the medium-modified mass and width of the Δ is given in Ref. [36], in terms of the nuclear density ρ. Writing $\widetilde{\Gamma}$ for the in-medium Δ width, one then has

$$\widetilde{\Gamma} = \Gamma_{\mathrm{Pauli}} - 2\Im(\Sigma_\Delta), \tag{38}$$

where Γ_{Pauli} is the Pauli-corrected width and Σ_Δ stands for the Δ self-energy. As a function of the nuclear density, the imaginary part of Σ_Δ can be parameterized as [36]

$$-\Im(\Sigma_\Delta) = C_{\mathrm{QE}}\left(\frac{\rho}{\rho_0}\right)^\alpha + C_{A2}\left(\frac{\rho}{\rho_0}\right)^\beta + C_{A3}\left(\frac{\rho}{\rho_0}\right)^\gamma. \tag{39}$$

The equilibrium density ρ_0 reflects the saturation density in the interior of finite nuclei. The terms with the coefficients C_{QE}, C_{A2}, and C_{A3} correspond to the processes $\Delta N \to \pi NN$, $\Delta N \to NN$, and $\Delta NN \to NNN$, respectively. Whereas C_{QE} enhances the number of Δ decays accompanied by a pion, the latter two contributions open up pionless decay channels through two- and three-body absorption mechanisms. The values of $C_{\mathrm{QE}}, C_{A2}, C_{A3}, \alpha, \beta$, and γ can be found in Refs. [36,53]. For our purposes, we

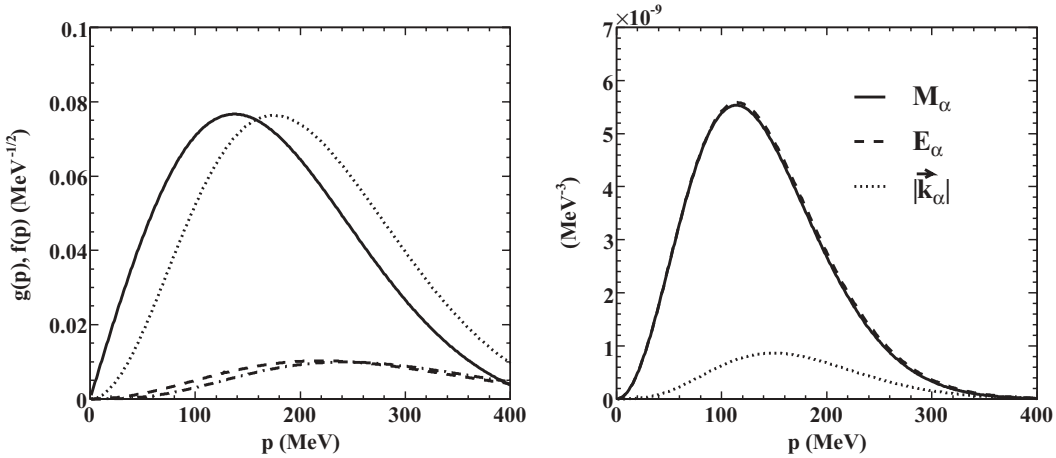

FIG. 3. The left panel shows the momentum wave functions for the carbon nucleus. The full (dashed) line corresponds to $g(p)$ [$f(p)$] for a $1s_{1/2}$ proton, the dotted (dash-dotted) line represents $g(p)$ [$f(p)$] for a $1p_{3/2}$ proton. In the right panel, the quantities defined in Eq. (36) are shown for a $1p_{3/2}$-shell ^{12}C proton.

shall adopt an average nuclear density $\rho = 0.75\rho_0$. Then, at the Δ peak, we calculate the following shifts

$$M_\Delta \longrightarrow M_\Delta + 30\ \text{MeV}, \qquad \Gamma \longrightarrow \Gamma + 40\ \text{MeV}. \tag{40}$$

In Ref. [54], a similar recipe was used to accommodate medium modifications in the calculation of ^{12}C(γ, pn) and ^{12}C(γ, pp) cross sections. There, the computations proved to compare favorably with the data in an energy regime where the reaction is dominated by Δ creation. It is worth stressing that photo-induced two-nucleon knockout reactions receive very small contributions from background diagrams, who form an important source of uncertainties when extracting resonance information.

IV. RESULTS AND DISCUSSION

In this section, we present computations for the process

$$\nu_\mu + p \overset{\Delta^{++}}{\rightarrow} \mu^- + p + \pi^+. \tag{41}$$

For scattering off a free nucleon, the strength of the process in Eq. (41) can be straightforwardly related to the other channels listed in Eq. (2) by applying the isospin relations of Eq. (3). In neutrino-nucleus scattering processes, these isospin relations can no longer be applied once pion rescatterings are considered. Indeed, charge-exchange effects are known to substantially affect the pionic final states due to side-feeding [40].

Unless otherwise stated, we use the vector form factors of Eqs. (13) and (14), the axial form factors of Eq. (16) with $M_A = 1.05$ GeV, and the $\Delta\pi N$ coupling defined in Eq. (18). For the RFG calculations, we adopt $k_F = 225$ MeV and an average binding energy of $E_B = 20$ MeV. The latter value can be considered as a fair estimate for the weighted average of the centroids of the single-particle strength distributions in typical even-even nuclei near the closed shells [55].

A. $WN\Delta$ and $\Delta\pi N$ couplings

Before discussing the nuclear effects described in Sec. III, we address some topics related to the elementary Δ couplings introduced in Sec. II B. Figure 4 assesses to what extent the extracted value for M_A is sensitive to the specific choice for the vector form factors. To this end, Fig. 4 compares the cross section computed with the Lalakulich fit of Eq. (15) and $M_A = 1.05$ GeV with the cross section computed with the $M1$-dominance form factors of Eqs. (13) and (14) and a 10% variation in the axial mass. To reach consistency between the two approaches, the axial mass used in the $M1$-dominance calculation needs to be 5–10% higher than the one that is used together with the Lalakulich fit. Consequently, analyzing data with the assumption of $M1$ dominance will generally lead to a 5–10% higher M_A value compared to an analysis using

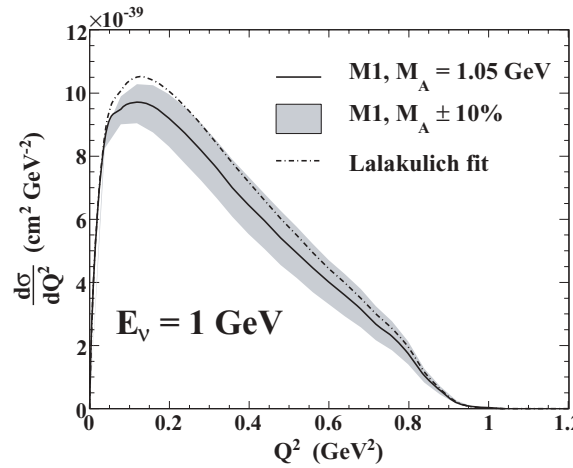

FIG. 4. Q^2 evolution of the cross section for $\nu_\mu + p \overset{\Delta^{++}}{\rightarrow} \mu^- + p + \pi^+$ at an incoming neutrino energy of 1 GeV. The full (dash-dotted) line corresponds to the vector form-factor parameterization of Eqs. (13) and (14) [Eq. (15)]. The shaded region indicates a 10% variation in the axial mass, using the same vector form factors as the full line.

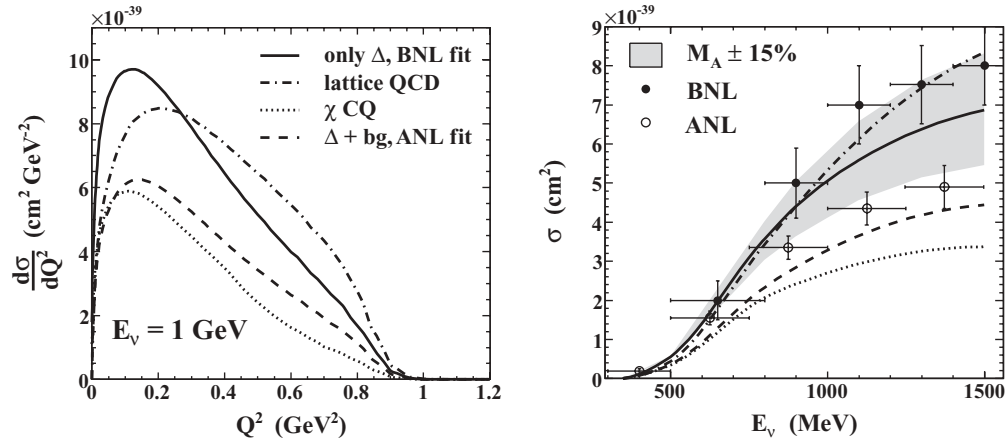

FIG. 5. Cross sections for $\nu_\mu + p \overset{\Delta^{++}}{\rightarrow} \mu^- + p + \pi^+$ with the $C_5^A(Q^2)$ contained in Fig. 2. In the left panel, Q^2 distributions are shown for $E_\nu = 1$ GeV. The dashed line represents a calculation with $C_5^A(0) = 0.867$ and $M_A = 985$ MeV [20]. In the right panel, the shaded region corresponds to a 15% variation in the axial mass. The solid (open) circles show BNL [56] (ANL [57]) total cross-section data.

the Lalakulich fit. This discrepancy is significant, as vector form factors are usually regarded as well known when they are used as input to extract the far less known axial form factors from neutrino-scattering data. Indeed, as pointed out in Sec. II B, the current situation for the axial-vector form factors is somewhat more dramatic. Figure 5 appraises the sensitivity of the Δ-production cross section to different parametrizations for the most important axial transition form factor, $C_5^A(Q^2)$. In the left panel, we contrast computations using a phenomenological result for $C_5^A(Q^2)$ with computations that employ the theoretical calculations shown in Fig. 2. Next to the fit to BNL data given in Eq. (16), the former involve a fit to ANL data within a model that includes background contributions, in addition to the Δ-pole mechanism [20]. Adopting the same Q^2 dependence as in Eq. (16), this leads to $C_5^A(0) = 0.867$ and $M_A = 985$ MeV [20]. Clearly, the Q^2 evolution of the Δ-production cross section exhibits a strong sensitivity to the adopted $C_5^A(Q^2)$ parametrization. Near $Q^2 = 0$, cross sections using the χCQ, QCD and background-model results are about 40% lower than the calculation with the Δ-dominance fit. This is almost entirely due to the difference in $C_5^A(0)$ values, which yields a ratio of $(0.9)^2/(1.2)^2 \approx 0.56$ for the dominant cross-section contribution. The soft $C_5^A(Q^2)$ predicted by the χCQ model results in cross sections that are much lower over the whole Q^2 range. However, the hard C_5^A form factor predicted by the QCD calculation leads to more strength toward higher Q^2 values. The ANL fit for C_5^A results in an integrated cross section that is about 30% lower than the calculation performed with the BNL fit. To put things in a more general perspective, the right panel of Fig. 5 makes a comparison between predictions based on different $C_5^A(Q^2)$ parametrizations and the available ANL and BNL total cross-section data. First, it should be noted that very large differences exist between the two data sets. For neutrino energies around 1 GeV, the BNL data exceed the ANL data by 30%. Within our Δ-dominance model and with the $C_5^A(Q^2)$ parametrization of Eq. (16), all data can be reasonably well covered if one admits a ±15% uncertainty on $M_A = 1.05$ GeV. Further, one can see that the lattice-QCD calculation for $C_5^A(Q^2)$ leads to a good description of the BNL cross-section data. However, the χCQ result underestimates both the BNL and ANL data. Finally, even though no background contributions are included here, the ANL fit for $C_5^A(Q^2)$ [20] only leads to a small underestimation of the ANL data by our Δ-dominance calculation, due to the large error flags. Hence, we deem that the current status of neutrino-scattering data does not allow an extraction of the axial form-factor parameters to a level better than 20–30%. To investigate the impact of different Δ-decay couplings, we have computed W distributions using both the traditional coupling of Eq. (18) and the Pascalutsa coupling of Eq. (22). The results are shown in Fig. 6, where it can be seen that differences between the two approaches are small. We infer an overall effect that does not exceed the 2% level.

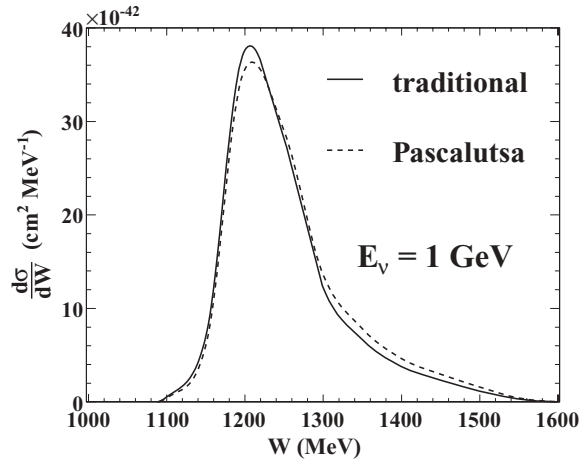

FIG. 6. Invariant-mass dependence of the cross section for $\nu_\mu + p \overset{\Delta^{++}}{\rightarrow} \mu^- + p + \pi^+$ at an incoming neutrino energy of 1 GeV. The hadronic invariant mass is defined as $W = \sqrt{m_N^2 + 2\omega m_N - Q^2}$. The full (dashed) line uses the $\Delta\pi N$ coupling of Eq. (18) [Eq. (22)].

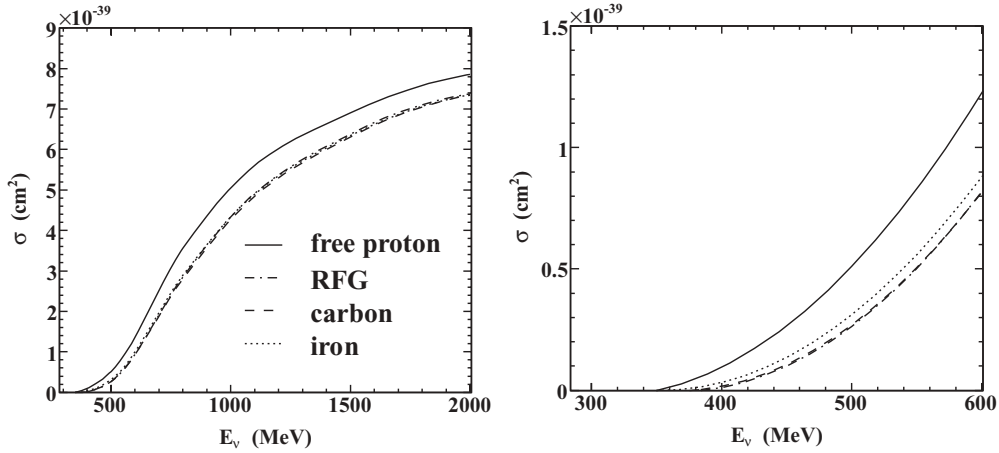

FIG. 7. Total cross sections per nucleon for $\nu_\mu + p \overset{\Delta^{++}}{\rightarrow} \mu^- + p + \pi^+$. The full line represents the elementary process, for scattering from a free proton. The dash-dotted line stands for the RFG calculations, whereas the dashed (dotted) line corresponds to scattering from a carbon (iron) target nucleus. The right panel focusses on the threshold region.

B. Nuclear-model effects: RPWIA vs. RFG

In this subsection, the results of Sec. IV A will be put in a more general perspective. To this end, we will compare neutrino-nucleus with neutrino-nucleon cross sections. Figure 7 shows how the total strength for the process in Eq. (41) varies with the incoming neutrino energy. Under the same kinematical conditions and with similar input for the Δ couplings, our results for the elementary process compare very well with the predictions published in Ref. [20]. Turning to the predictions for target nuclei, Fig. 7 shows how the elementary cross section is halved near threshold. For higher incoming energies, the effect dwindles to 20% at $E_\nu = 800$ MeV and 8% at $E_\nu = 2$ GeV. The RFG calculations are in good to excellent agreement with both the carbon and iron RPWIA results. The only discernable feature of Fig. 7 is that the iron curve exceeds the carbon and RFG ones by roughly 15% just beyond threshold. This can be understood after recognizing that the iron result is largely due to outer-shell protons, which are less bound than the corresponding carbon ones. Also, the adopted binding-energy value for the RFG calculations is close to the weighted binding energy per nucleon in a carbon nucleus, explaining the close agreement between these two cases. Clearly, the $\nu_\mu A$ cross sections are very sensitive to binding-energy differences at lower incoming energies. These effects, however, vanish at higher neutrino energies and are of the order of 1% at $E_\nu =$ 1 GeV. As a matter of fact, at sufficiently high energies RFG calculations with a well-chosen binding-energy correction are almost indiscernible from the corresponding RPWIA results. These findings are assessed in more detail in Figs. 8, 9, and 10. Figures 8 and 9 compare RFG and RPWIA computations. The former considers scattering from a carbon target at $E_\nu = 800$ MeV, which corresponds to the mean energy of the neutrino beam used by the MiniBooNE experiment. As can be appreciated from Fig. 8, the RFG and RPWIA models produce almost identical results. In Fig. 9, we present the ratio of RFG to carbon RPWIA results for the twofold cross section $d^2\sigma/dT_\pi d\cos\theta_\pi^*$, where T_π is the produced pion's kinetic energy and θ_π^* its direction relative to the neutrino-beam. In the threshold region, cross sections are extremely small and subject to large fluctuations. Beyond threshold, however, differences between the RFG and RPWIA result do not exceed the 5% level over the whole (T_π, θ_π^*) range. Consequently, on integrating over T_π and θ_π^*, we find that the total RFG cross section exceeds the RPWIA one by about 2%. Figure 10 compares the cross section for a carbon nucleus with the one for an iron nucleus at $E_\nu = 1.5$ GeV. Although the total strength, integrated over the outgoing muon energy E_l, is the same for both nuclei, it is interesting to note that the iron distribution is shifted with respect to the carbon cross section. Again, this reflects the fact that on average it requires more energy to knock a proton out of a carbon nucleus than out of an iron nucleus, leaving therefore less energy for the outgoing muon.

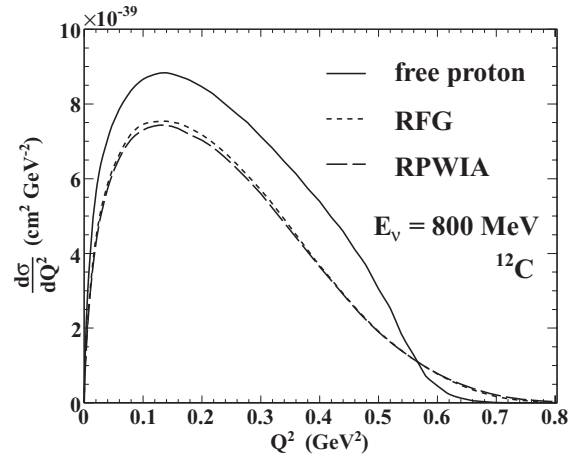

FIG. 8. Cross section per nucleon for $\nu_\mu + p \overset{\Delta^{++}}{\rightarrow} \mu^- + p + \pi^+$ on carbon at an incoming neutrino energy of 800 MeV. The full line represents the elementary process, whereas the short-dashed (long-dashed) line stands for the RFG (RPWIA) calculation.

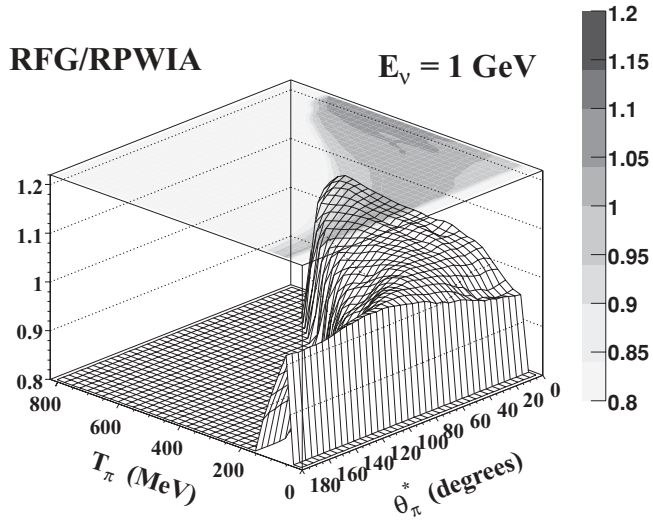

FIG. 9. Ratio of RFG to RPWIA computations for the $d^2\sigma/dT_\pi d\cos\theta^*_\pi$ cross section of the process $\nu_\mu + p \overset{\Delta^{++}}{\rightarrow} \mu^- + p + \pi^+$. A carbon target and an incoming neutrino energy of 1 GeV are considered.

C. Primary pion production and inclusive observables

An important test for any nuclear model lies in the comparison with inclusive electron-nucleus-scattering data. In Fig. 11, we compare RPWIA calculations for primary one-pion production to Anghinolfi data [58] for electron scattering off an oxygen target. As the intermediate Δ resonance is created inside an oxygen nucleus, we have now also applied the medium modifications given in Eq. (40) to the mass and width in the denominator of the Δ propagator. For further comparison, we have included Δ-production calculations performed in the framework of Lalakulich *et al.* [59], using the same nuclear-physics input as our RPWIA calculations. To separate the one-pion contribution (1-π) from the full inclusive cross section (*incl*), we have employed the scheme proposed in Ref. [38] and also applied in Refs. [39,60]. Recognizing that the inclusive cross section is proportional to the free Δ decay width, one can either use the full medium corrections or add only the terms that relate to the pion decay channel, represented by the $C_{\rm QE}$ term in Eq. (39), to the width in the numerator. As a result, using the parametrizations found in Refs. [36,53], again with $\rho = 0.75\rho_0$ and at the Δ peak, we find that the free decay width receives no appreciable medium corrections with respect to the one-pion decay channel. Hence, the full and one-pion computations in Fig. 11 are obtained by applying the medium modifications of Eq. (40) in the denominator and, at the same time, adding the values of 40 MeV (full) and 0 MeV (one-pion) to the width in the numerator of the inclusive cross section. Compared to the data, the peak of the displayed cross sections is moved toward higher energy transfers. Moreover, the inclusive strength in the Δ region is underestimated. These observations may point to the importance of nonresonant background contributions [41], which are not taken into account in this discussion. Contrasting the calculations of Ref. [59], it is seen that the one-pion contribution comprises about 75–80% of the full inclusive

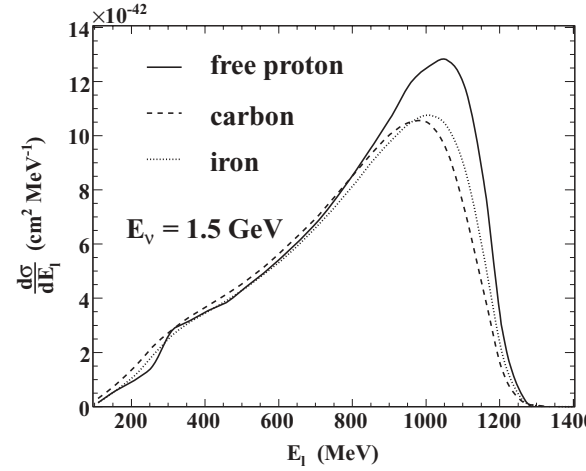

FIG. 10. The $\nu_\mu + p \overset{\Delta^{++}}{\rightarrow} \mu^- + p + \pi^+$ cross section per nucleon as a function of the lepton energy E_l for $E_\nu = 1.5$ GeV. The full line represents the elementary process, whereas the dashed (dotted) line refers to scattering from carbon (iron).

result. The remainder of the strength resides in pionless decay modes, which have become available as additional decay channels due to two- and three-body absorption processes such as $\Delta N \rightarrow NN$ and $\Delta NN \rightarrow NNN$. However, the major difference between the one-pion calculation of Ref. [59] and the ones presented in this work lies in the Δ propagator and the use of a $\Delta\pi N$ decay vertex in the latter. Using the free value $f_{\pi N\Delta} = 2.21$, it is observed that our result for primary one-pion production agrees well with the one-pion result of Ref. [59] for energy transfers up to the Δ peak. For larger ω, however, both of the Ref. [59] calculations are considerably smaller. There, the explicit inclusion of the $\Delta\pi N$ decay vertex

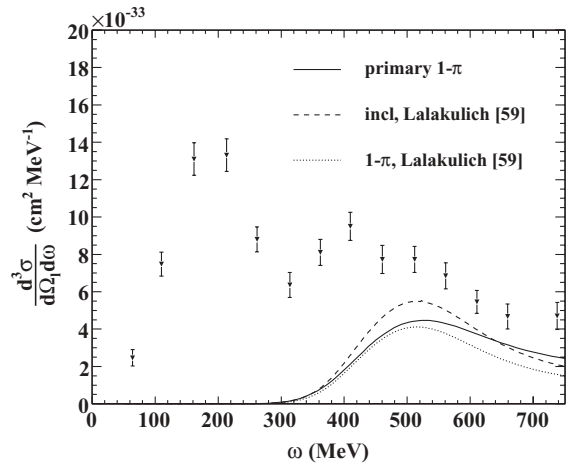

FIG. 11. Comparison of cross-section calculations to inclusive electron-scattering data. Shown is $d^3\sigma/d\Omega_l d\omega$ against energy transfer ω, for scattering off an oxygen target at an incoming electron energy of $E_e = 1080$ MeV and an electron scattering angle of $\theta_{e'} = 32^\circ$. The full line represents the primary Δ-mediated one-pion production strength, as computed in our RPWIA model with Δ medium modifications. The dashed (dotted) line denotes a calculation of Δ production (the one-pion part of Δ production) carried out in the framework of Ref. [59]. Data points are taken from Refs. [58,61].

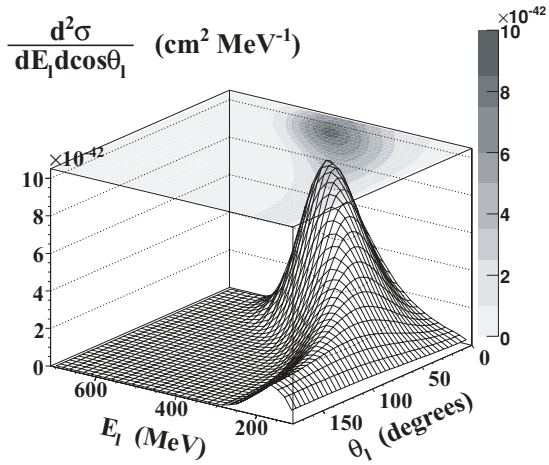

FIG. 12. Cross section per nucleon for $\nu_\mu + p \overset{\Delta^{++}}{\rightarrow} \mu^- + p + \pi^+$ as a function of outgoing-muon energy and scattering angle. The incoming neutrino energy is 800 MeV, the target nucleus is carbon.

and the detailed treatment of the Δ propagator (instead of the Breit-Wigner form used in Ref. [59]) seem to account for a better agreement with data. Although our calculation for primary one-pion production could never be measured as a separate contribution in the Δ region, it can be safely concluded that it gives a good estimate of the Δ-mediated one-pion yield.

To put our calculations in a more general perspective, we make a comparison with other theoretical efforts on inclusive lepton scattering off nuclei, as, for example, presented in Ref. [41]. There, the nucleus is described as a local Fermi gas of nucleons. The lepton-nucleus interaction is treated in the IA, and special attention is paid to including in-medium effects on the pion-production mechanisms. In the middle panel of Fig. 2 in Ref. [41], the total Δ-production contribution is shown for electron scattering off an oxygen target at the same kinematics as in Fig. 11 of this work. Compared to the one-pion calculations presented here, one can see that the inclusion of pionless decay modes shifts the peak of the Δ contribution to lower energy transfers. Indeed, because no pion needs to be created, the pionless decay modes contribute strength in the low $W(\sim$low $\omega)$ region.

In view of recent results presented by the MiniBooNE and K2K Collaborations [3], we conclude this section with some computations for the specific neutrino energies and target nuclei employed by these experiments. From an experimental viewpoint, the most accessible distributions are the ones with respect to outgoing-muon variables. Figure 12 depicts an RPWIA calculation, including Δ medium modifications, for a twofold differential cross section against the outgoing-muon energy and scattering angle with respect to the neutrino beam. The incoming neutrino energy is fixed at 800 MeV, corresponding to MiniBooNE's mean beam energy. Because MiniBooNE has carbon as target material, this calculation was performed on a carbon nucleus. The result shown in Fig. 12 can be integrated over θ_l or E_l to yield the one-fold cross sections displayed in Fig. 13. For comparison, we have also computed the free cross section and the basic RPWIA one, which does not take into account Δ medium modifications. Relative to the free cross section, the RPWIA angular distribution for a carbon target is reduced by about 20%. In general, the outgoing muon prefers a forward direction, although a minor shift seems to take place between the free and the bound case. This effect relates to the change in the muon-energy distribution, depicted in the right-hand panel of Fig. 13. Indeed, for scattering off bound protons, one observes a shift of the E_l distribution toward lower values. Recognizing the correlation between high muon energies and forward scattering angles, as can be appreciated in Fig. 12, the bound case will correspondingly yield a larger number of events at slightly higher scattering angles. We also note that the RPWIA result fades out sooner than the elementary cross section, because a certain amount of energy is needed to knock the carbon proton out of its shell. Further, Fig. 13 shows that the inclusion of Δ medium modifications results in a 50% reduction of the basic RPWIA calculations. In addition, the muon-energy distribution is shifted toward lower E_l, by an amount that corresponds to the mass shift in Eq. (40). In Ref. [38], a similar effect is observed

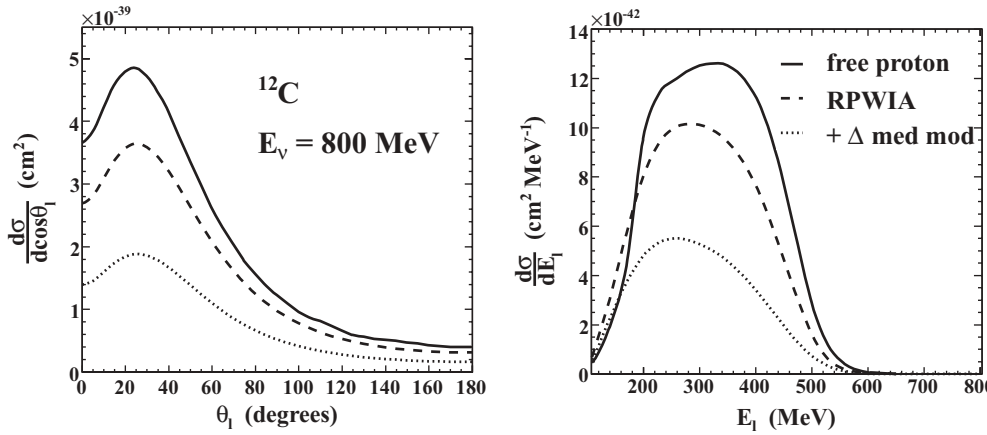

FIG. 13. Cross sections per nucleon for $\nu_\mu + p \overset{\Delta^{++}}{\rightarrow} \mu^- + p + \pi^+$, for 800-MeV neutrinos scattering from a carbon target. The left (right) panel shows the cross section as a function of the outgoing-muon scattering angle (energy). Each of the panels contrasts the elementary cross section (full line) with the RPWIA result, shown with (dotted) and without (dashed) Δ medium modifications.

in the case of electron-neutrinos scattering off oxygen. There, the authors infer a 40% reduction of Δ-mediated one-pion production, due to medium-modification effects. Moreover, of particular interest in relation to our work are the results shown in Fig. 1 of Ref. [38]. In that figure, a distinction is made between the total Δ-production cross section and the fraction of Δs that eventually produces pions. They observe that only ∼80% of the Δs that are created inside an oxygen nucleus produce pions. The rest is categorized as QE-like, because of the pionless decay modes it corresponds to. From their results, it also follows that these QE-like events mainly contribute in the region of high outgoing-lepton energy. These findings corroborate with our previous results for inclusive electron scattering.

V. CONCLUSION AND OUTLOOK

We have developed a relativistic framework to study Δ-mediated one-pion production from nuclei at medium energies. The proposed formalism offers great flexibility in calculating various observables both for the free process and for scattering from nuclear targets. Motivated by operational and planned experiments, we have conducted a systematic study by addressing the impact of Δ-coupling ambiguities on Q^2 and W distributions and total cross sections. Cross sections are found to vary by as much as 10% depending on whether the $M1$-dominance assumption is used to extract the vector form factors. We infer that a data analysis that assumes $M1$ dominance will generally lead to a 5–10% higher value for the axial mass M_A compared to an analysis that employs a direct fit to electroproduction helicity amplitudes. Uncertainties in the dominant axial form factor $C_5^A(Q^2)$ arising from model-dependent analyses of bubble-chamber data have a substantial effect on the Δ-production cross sections. Cross sections computed with a $C_5^A(Q^2)$ parametrization derived from a Δ-dominance analysis of the BNL Q^2 distribution are found to be 30% larger than the ones that use a fit to ANL data within a model that also includes background contributions. Within our Δ-dominance model, the present status of neutrino-scattering data places ±15% uncertainties on the value $M_A = 1.05$ GeV. In the W distribution, we observe 2%-level deviations between the traditional Δ-decay coupling choice and a consistent one, which effects a decoupling from the spin-1/2 terms.

To investigate the influence of nuclear effects, we have computed RPWIA neutrino-nucleus cross sections for carbon, oxygen, and iron nuclei. Using a prescription that gives good results in photo-induced two-nucleon knockout and electron-scattering studies, we infer a 50% suppression of the RPWIA primary one-pion cross sections due to medium effects. The nuclear responses are very sensitive to binding-energy differences at lower neutrino energies. From $E_\nu = 1$ GeV onward, the cross sections per nucleon for different nuclear targets are seen to agree at the 1% level. As an application, we have produced predictions for the Δ-mediated one-pion contribution to lepton-nucleus scattering. Compared to the electron-scattering data, we underestimate the strength in the Δ region, observing the largest discrepancies in the low-ω region. These differences can be understood after recognizing that we do not include pionless decay modes in our calculations.

To assess the nuclear-model uncertainty in our description of Δ-mediated one-pion production, we have also contrasted the RPWIA results with calculations performed within an RFG model with a well-considered binding-energy correction. At 1-GeV neutrino energies, differences between one- and twofold distributions computed within both models do not exceed the 5% level. The agreement is better for total cross sections, where deviations between the RFG and RPWIA model dwindle to 1–2%. Hence, for sufficiently high incoming neutrino energies, the influence of Fermi motion, nuclear binding, and the Pauli exclusion principle can be well described by adopting an RFG model with binding-energy correction. The RFG model, however, just as the RPWIA approach, falls short in implementing FSI and nuclear correlations of the short- and long-range type. Contrary to the RFG, the model proposed in this work has the important advantage that it can serve as a starting point for a relativistic and quantum-mechanical study of FSI mechanisms. As a matter of fact, the inclusion of FSI for the ejected pions and nucleons is currently under study. To this end, we closely follow the lines of Ref. [51], where use is made of a relativistic Glauber model for fast ejectiles and an optical-potential approach for lower ejectile energies.

ACKNOWLEDGMENTS

The authors acknowledge financial support from the Research Foundation-Flanders (FWO) and the Research Council of Ghent University.

[1] (BooNE Collaboration) home page http://www-boone.fnal.gov/.
[2] (K2K Collaboration) home page http://neutrino.kek.jp/.
[3] R. Tayloe (MiniBooNE Collaboration), in *Proceedings of NuInt07: the 5th International Workshop on Neutrino-Nucleus Interactions in the Few-GeV Region, Batavia, 2007*, edited by G. P. Zeller, J. G. Morfin, and F. Cavanna (AIP, Melville, New York, 2007), p. 39; L. Whitehead and A. Rodriguez (K2K Collaboration), *ibid.* p. 169.
[4] S. Nakayama *et al.* (K2K Collaboration), Phys. Lett. **B619**, 255 (2005).
[5] M. Hasegawa *et al.* (K2K Collaboration), Phys. Rev. Lett. **95**, 252301 (2005).
[6] R. Gran *et al.* (K2K Collaboration), Phys. Rev. D **74**, 052002 (2006).
[7] A. A. Aguilar-Arevalo *et al.* (MiniBooNE Collaboration), Phys. Lett. **B664**, 41 (2008).
[8] A. A. Aguilar-Arevalo *et al.* (MiniBooNE Collaboration), Phys. Rev. Lett. **100**, 032301 (2008).
[9] S. Boyd (MINERνA Collaboration), Nucl. Phys. Proc. Suppl. **139**, 311 (2005).
[10] (SciBooNE Collaboration) home page http://www-sciboone.fnal.gov/.
[11] S. L. Adler, Ann. Phys. (NY) **50**, 189 (1968).
[12] C. H. Llewellyn Smith, Phys. Rep. **3**, 261 (1972).

[13] P. A. Schreiner and F. Von Hippel, Phys. Rev. Lett. **30**, 339 (1973).
[14] D. Rein and L. M. Sehgal, Ann. Phys. (NY) **133**, 79 (1981).
[15] K. M. Graczyk and J. T. Sobczyk, Phys. Rev. D **77**, 053001 (2008).
[16] O. Lalakulich and E. A. Paschos, Phys. Rev. D **71**, 074003 (2005).
[17] O. Lalakulich, E. A. Paschos, and G. Piranishvili, Phys. Rev. D **74**, 014009 (2006).
[18] L. Alvarez-Ruso, S. K. Singh, and M. J. Vicente Vacas, Phys. Rev. C **59**, 3386 (1999).
[19] T. Sato, D. Uno, and T. S. H. Lee, Phys. Rev. C **67**, 065201 (2003).
[20] E. Hernández, J. Nieves, and M. Valverde, Phys. Rev. D **76**, 033005 (2007).
[21] K. S. Kuzmin, V. V. Lyubushkin, and V. A. Naumov, Acta Phys. Pol. B **37**, 2337 (2006).
[22] D. Barquilla-Cano, A. J. Buchmann, and E. Hernández, Phys. Rev. C **75**, 065203 (2007).
[23] C. Alexandrou, Th. Leontiou, J. W. Negele, and A. Tsapalis, Phys. Rev. Lett. **98**, 052003 (2007).
[24] C. Alexandrou, G. Koutsou, Th. Leontiou, J. W. Negele, and A. Tsapalis, Phys. Rev. D **76**, 094511 (2007).
[25] L. S. Geng, J. M. Camalich, L. Alvarez-Ruso, and M. J. Vicente Vacas, Phys. Rev. D **78**, 014011 (2008).
[26] L. S. Geng, J. Martin Camalich, L. Alvarez-Ruso, and M. J. Vicente Vacas, Mod. Phys. Lett. A **23**, 2246 (2008).
[27] M. Procura, Phys. Rev. D **78**, 094021 (2008).
[28] V. Pascalutsa and R. Timmermans, Phys. Rev. C **60**, 042201(R) (1999).
[29] C. J. Horowitz, H. Kim, D. P. Murdock, and S. Pollock, Phys. Rev. C **48**, 3078 (1993).
[30] W. M. Alberico, M. B. Barbaro, S. M. Bilenky, J. A. Caballero, C. Giunti, C. Maieron, E. Moya de Guerra, and J. M. Udías, Nucl. Phys. **A623**, 471 (1997).
[31] M. C. Martínez, P. Lava, N. Jachowicz, J. Ryckebusch, K. Vantournhout, and J. M. Udías, Phys. Rev. C **73**, 024607 (2006).
[32] O. Benhar, A. Fabrocini, S. Fantoni, and I. Sick, Nucl. Phys. **A579**, 493 (1994).
[33] O. Benhar, N. Farina, H. Nakamura, M. Sakuda, and R. Seki, Phys. Rev. D **72**, 053005 (2005).
[34] O. Benhar and D. Meloni, Nucl. Phys. **A789**, 379 (2007).
[35] A. M. Ankowski and J. T. Sobczyk, Phys. Rev. C **77**, 044311 (2008).
[36] E. Oset and L. L. Salcedo, Nucl. Phys. **A468**, 631 (1987).
[37] H. Kim, S. Schramm, and C. J. Horowitz, Phys. Rev. C **53**, 2468 (1996).
[38] S. K. Singh, M. J. Vicente-Vacas, and E. Oset, Phys. Lett. **B416**, 23 (1998).
[39] S. Ahmad, M. S. Athar, and S. K. Singh, Phys. Rev. D **74**, 073008 (2006).
[40] T. Leitner, L. Alvarez-Ruso, and U. Mosel, Phys. Rev. C **73**, 065502 (2006).
[41] O. Buss, T. Leitner, U. Mosel, and L. Alvarez-Ruso, Phys. Rev. C **76**, 035502 (2007).
[42] L. Alvarez-Ruso, L. S. Geng, S. Hirenzaki, and M. J. Vicente Vacas, Phys. Rev. C **75**, 055501 (2007).
[43] R. J. Furnstahl, B. D. Serot, and H.-B. Tang, Nucl. Phys. **A615**, 441 (1997).
[44] P. Lava, N. Jachowicz, M. C. Martínez, and J. Ryckebusch, Phys. Rev. C **73**, 064605 (2006).
[45] C. Praet, N. Jachowicz, J. Ryckebusch, P. Vancraeyveld, and K. Vantournhout, Phys. Rev. C **74**, 065501 (2006).
[46] N. Jachowicz, P. Vancraeyveld, P. Lava, C. Praet, and J. Ryckebusch, Phys. Rev. C **76**, 055501 (2007).
[47] J. Bjorken and S. Drell, *Relativistic Quantum Mechanics* (McGraw-Hill, New York, 1964).
[48] P. Stoler, Phys. Rep. **226**, 103 (1993).
[49] A. J. Dufner and Y. S. Tsai, Phys. Rev. **168**, 1801 (1968).
[50] E. A. Paschos, J.-Y. Yu, and M. Sakuda, Phys. Rev. D **69**, 014013 (2004).
[51] W. Cosyn, M. C. Martínez, and J. Ryckebusch, Phys. Rev. C **77**, 034602 (2008).
[52] S. Gardner and J. Piekarewicz, Phys. Rev. C **50**, 2822 (1994).
[53] J. Nieves, E. Oset, and C. Garcia-Recio, Nucl. Phys. **A554**, 554 (1993).
[54] I. J. D. MacGregor *et al.*, Phys. Rev. Lett. **80**, 245 (1998).
[55] K. L. G. Heyde, *The Nuclear Shell Model* (Springer-Verlag, Berlin, 1994).
[56] T. Kitagaki *et al.*, Phys. Rev. D **34**, 2554 (1986).
[57] G. M. Radecky *et al.*, Phys. Rev. D **25**, 1161 (1982).
[58] M. Anghinolfi *et al.*, Nucl. Phys. **A602**, 405 (1996).
[59] O. Lalakulich, N. Jachowicz, C. Praet, and J. Ryckebusch, Phys. Rev. C **79**, 015206 (2009).
[60] M. S. Athar, S. Ahmad, and S. K. Singh, Phys. Rev. D **75**, 093003 (2007).
[61] O. Benhar, D. Day, and I. Sick, nucl-ex/0603032.